# UC San Diego
## UC San Diego Previously Published Works

**Title**
Centrifuge Modeling of Energy Foundations

**Permalink**
https://escholarship.org/uc/item/38m3q1xk

**ISBN**
9781848215726

**Author**
McCartney, John S

**Publication Date**
2013-08-30

**DOI**
10.1002/9781118761809.ch5

Peer reviewed

eScholarship.org Powered by the California Digital Library
University of California

Chapter 5

# Centrifuge Modeling of Energy Foundations

## 5.1. Introduction

Although incorporation of heat exchangers into deep foundation elements (energy foundations) helps reduce the installation costs of ground-source heat exchange systems [BRA 98; ENN 01; BRA 06], an issue encountered is the potential for foundation movements due to thermal expansion and contraction of the foundation element or surrounding soil. Further, soil-structure interaction may restrain movement of the foundation, leading to generation of thermally induced stresses. Thermo-mechanical soil-structure interaction has been documented in several field-scale case histories [LAL 06; BOU 09; LAL 11; AMA 12; MCC 12]. Although thermo-mechanical soil-structure interaction analyses permit prediction of changes in axial stress or strain during heating and cooling operations [KNE 11; PLA 12], they require empirical data for calibration of model parameters and verification of predictions. This is especially the case when considering the behavior of energy piles in some soil deposits, such as soft clays or unsaturated soils. Centrifuge modeling is a useful approach to measure empirical parameters for soil-structure interaction analyses for energy foundations, as the properties of scale-model foundations and soil layers can be carefully controlled and different configurations can be considered for lower costs that full-scale field testing. An additional benefit of centrifuge modeling is that scale-model energy foundations can be loaded to failure to characterize the effects of temperature on the load-settlement curve. The back-calculated ultimate side shear distribution and end bearing are useful parameters for soil-structure interaction analyses. Further, centrifuge tests on scale-model foundations with embedded instrumentation permit measurement of thermally induced stresses and strains in the foundation, which can be used to validate soil-structure interaction analyses or finite element models. Areas of

thermo-mechanical soil-structure interaction analysis being explored in the centrifuge are the impact of thermally induced radial stresses on the side shear resistance, end boundary condition (foundation toe and head) effects, and the impact of temperature on the stress-strain curves for end bearing and side shear resistance.

This chapter includes a review of the relevant scaling relationships and strategies to account for issues with scaling heat transfer in the centrifuge, the details of scale-model energy foundation development, and the procedures and typical results from tests used to define parameters for soil-structure interaction analyses. The tests discussed in this chapter focus on the behavior of semi-floating (i.e., the toe of the foundation is resting in soil) energy foundation models in unsaturated silt.

## 5.2. Background on Thermo-Mechanical Soil-Structure Interaction

As an energy foundation is heated or cooled, it may expand or contract, respectively, depending on the end-restraint boundary conditions. For unconstrained conditions, the axial thermal strain can be calculated as follows:

$$\varepsilon_{T,free} = \alpha_c \Delta T \quad [5.1]$$

where $\alpha_c$ is the coefficient of linear thermal expansion of reinforced concrete, and $\Delta T$ is the change in temperature. Thermal strain is defined as positive for compression. Accordingly, $\alpha_c$ is negative as structural elements expand during heating (positive $\Delta T$). The coefficient of thermal expansion of unreinforced concrete ranges from -9 to -14.5 με/°C depending on the aggregate mineralogy, while that of the steel reinforcements ranges from -11.9 to -13 με/°C [BOU 09; STE 12]. Because these materials are relatively compatible, significant differential thermal strains are not expected in reinforced concrete. The value of $\varepsilon_{T,free}$ is an upper limit on the thermal strains due to heating or cooling. For constrained conditions, the actual thermal strains will be less than those predicted by Eq. 5.1. In this case, the thermal axial stresses induced in an energy foundation can be calculated as follows:

$$\sigma_T = E\left(\varepsilon_T - \alpha_c \Delta T\right) \quad [5.2]$$

where E is the Young's modulus of reinforced concrete and $\varepsilon_T$ is the actual thermal strain. For real energy foundations embedded in soil or rock, soil-structure interaction mechanisms will restrict the movement of the foundation during heating. Specifically, the side shear resistance, end bearing, and stiffness restraint of the overlying building will lead to different distributions in thermally induced stresses and strains in an energy foundation [LAL 06; BOU 09; AMA 12; MCC 12].

## 5.3. Centrifuge Modeling Concepts

Centrifuge modeling relies on the concept of geometric similitude, which assumes that a full-scale prototype soil layer will have the same stress state as a model-scale soil layer that is N times smaller when spinning in a geotechnical centrifuge at a centripetal acceleration that is N times larger than that of earth's gravity [KO 88; TAY 95]. The centripetal acceleration generates an increased body force field in the scale-model. Geometric similitude can be employed to extrapolate the load-settlement behavior and thermal soil-structure interaction phenomena of scale-model energy foundations to those representative of full-scale prototype foundations in the real world. After scaling the length of the foundation by a factor of 1:N (model:prototype), strains in the foundation scale by a factor of 1:1, and forces scale by a factor of $1:N^2$ [KO 88; TAY 95]. One issue in modeling energy foundations is that the temperature does not depend on the increased body forces in the centrifuge. Spatial measurements of temperature in dry quartz sand surrounding a cylindrical heat source during centrifugation at different g-levels by Krishnaiah and Singh [KRI 04] confirm that centrifugation does not lead to a change in the heat flow process. However, if the dimensions associated with the spatial distribution of heat flow were scaled from model to prototype scale (assuming the same thermal conductivity in both cases), the time required for heat flow by conduction would be $N^2$ times faster in the centrifuge model ($1:N^2$). Saviddou [SAV 88] derived this scaling factor from the diffusion equation, which only includes scaling of the length. An implication of temperature scaling is that a greater volume of soil surrounding the model-scale foundation will be affected by changes in temperature. Soils change in volume with temperature, so if a greater zone of soil around the foundation is affected then the effects of differential volume change of the foundation and soil may be emphasized. From this perspective, centrifuge modeling will provide a worst-case scenario. A solution to address the scaling issue is to calibrate numerical simulations of the tests using the data from model scale. However, if the goal of testing is to evaluate the impact of temperature on the load-settlement curve of the foundations, time should be provided to reach steady-state conditions. However, if the goal is to evaluate the impact of temperature on the axial strain distribution in the foundation, tests can be performed until strains stabilize while the foundation temperature is held constant. This amount of time depends on the soil type.

## 5.4. Centrifuge Modeling Components

### 5.4.1. *Centrifuge Model Fabrication and Characterization*

Two scale-model, semi-floating energy foundations are evaluated in this chapter. The first (Foundation A) is a simple foundation suitable for evaluation of the impact of temperature on the load-settlement curve of the foundation, while the second

(Foundation B) contains embedded instrumentation making it suitable for evaluation of the impact of temperature on the stress-strain distribution in the reinforced concrete. Both model foundations have lengths of 381 mm, but Foundation A has a diameter of 76.2 mm while Foundation B has a smaller diameter of 50.8 mm. Both foundations were tested at a g-level of 24, so they represent prototype drilled shafts having lengths of 9.1 m and diameters of 1.8 and 1.2 m, respectively. Schematics of the foundations are shown in Figure 5.1.

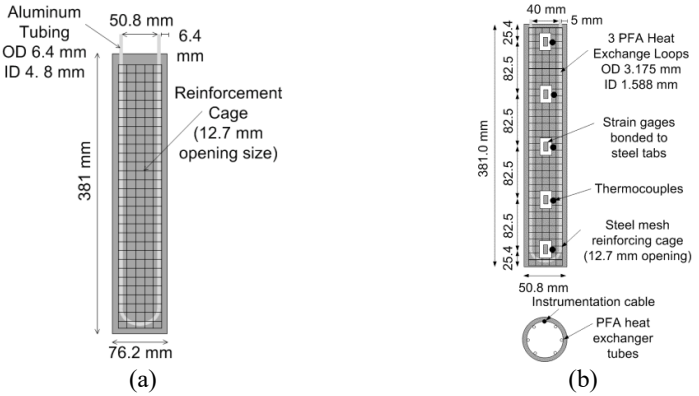


**Figure 5.1.** *Scale-model energy foundations: (a) Foundation A; (b) Foundation B*

Although drilled shafts are typically cast in place in the soil, the model energy foundations were precast outside of the soil layer due to the large amount of instrumentation, cables, and heat exchanger tubing. This also permits the foundations to be reused in subsequent tests, and to be tested outside of the soil layer to characterize their thermal and mechanical properties. The foundations were formed by pouring concrete into a cardboard tube containing the reinforcement cage. The fine aggregate was uniform sand with a particle size of 0.5 mm, while the coarse aggregate was gravel having a maximum particle size less than 6 mm (to permit flow through the reinforcement cage openings). Foundation A contained a single aluminum heat exchanger tube with relatively large diameter attached to the inside of the reinforcement cage, while Foundation B contained three small-diameter, high density Perfluoroalkoxy (PFA) tubing loops attached to the inside of the reinforcement cage. The use of 3 loops in Foundation B permits more uniform distribution of heat. Foundation B contains 5 strain gages bonded to steel tabs embedded in the concrete, with thermocouples installed at the same locations. The gages were selected because their coefficient of thermal expansion was similar to that of steel, and because they have a stable response to cyclic heating and cooling. The gages were first attached with temperature resistant M-Bond AE-15 adhesive to

30 mm-long steel tabs having a dog-bone shape with a hole punched at either end. This adhesive was chosen because it should be cured at an elevated temperature of 85 °C, making it less likely to slip during cyclic heating and cooling than other adhesives that cure at room temperature.

A comprehensive set of characterization tests were performed on Foundation B outside of the soil in a load frame at 1-gravity to determine the mechanical and thermal properties of the reinforced concrete. These results from these tests are reported in detail by Stewart [STE 12]. The first test involved application of incremental axial loads under room temperature conditions, taking care to properly level the foundation and center the load to avoid bending. The Young's modulus determined using the strain gauge data and a linearly variable deformation transformer (LVDT) was 7.17 GPa. This is soft compared to the Young's modulus of concrete in drilled shafts (approximately 30 GPA) due to the smaller aggregate size. The foundation was then heated to a temperature of 62 °C by circulating fluid through the heat exchange tubes within the foundation. The foundation was permitted to freely expand under this axial stress, permitting definition of the coefficient of linear thermal expansion of the reinforced concrete ($\alpha_c$ = -7.5 με/°C, where με is micro-strain). The thermal response of each strain gauge was different, likely due to differences in curing of the adhesive bonding the strain gages to the steel tabs. However, because the thermal strain should theoretically be the same at each location along the length of the foundation for free expansion, thermal correction factors were defined using the reading from the LVDT. Before application of any correction factors, the gages were corrected for the thermal offset error specific to this batch of gages and for differential expansion of the steel tabs (measured to be $\alpha_s$ = -8.5 με/°C) and reinforced concrete [STE 12].

### 5.4.2. *Experimental Setup*

A schematic of the containers used for testing of Foundations A and B are shown in Figures 5.2(a) and 5.2(b), respectively. In both cases, the container is a cylindrical aluminum tank with an inside diameter of 0.6 m, wall thickness of 13 mm, and a height of 0.54 m. A 13 mm-thick insulation sheet was wrapped around the container to prevent heat transfer through the sides of the cylinder (no-flow boundary). The bottom of the container permits some loss of heat, but it was preferred not to install insulation beneath the container to provide a stiff platform for loading. Loads were applied to the foundations using a horizontally-mounted, brushed DC electric motor with a coupling to a vertical worm drive. The motor is mounted on a reaction frame. Applied loads were measured using a load cell attached to the shaft of the worm drive, and a National Instruments motor control module was used to maintain a constant load using a force-feedback control loop. Additional pictures of the container and load frame are shown in Stewart [STE 12]. The configurations of the tests were slightly different. The goal of the tests on Foundation A was to measure

the impact of temperature on the load-settlement curve, so four foundations were installed in the same container so that they would have nearly identical soil conditions. The spacing in Figure 5.2(a) led to minimal interference between foundations with respect to thermal and mechanical loading. The goal of the tests on Foundation B was to characterize stress-strain distributions for validation of numerical simulations, so the foundation was placed in the middle of the container.

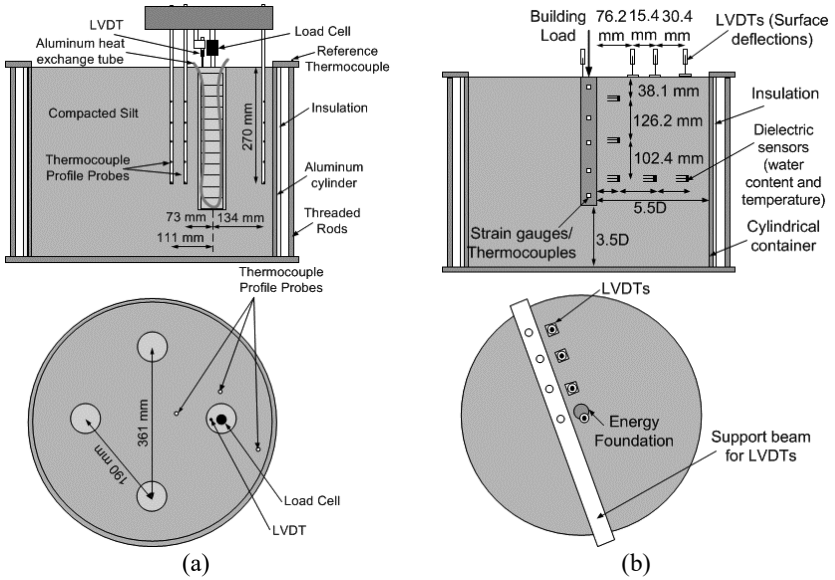


**Figure 5.2:** *Centrifuge-scale testing setups: (a) For evaluating the capacity of energy foundations; (b) For evaluating thermally induced strain distributions*

The location of instrumentation incorporated into the centrifuge containers are shown in Figure 5.2. An LVDT was placed on top of the foundation. The LVDTs were mounted on cantilever arms connected to a support beam across the top of the container. Three thermocouple profile probes were inserted into the soil at different radial locations around Foundation A. These probes were used to measure transient changes in temperature of the soil surrounding the foundation to assess heat transfer processes. Dielectric sensors (model EC-TM from Decagon Devices), capable of inferring the volumetric water content and temperature of the soil, were placed in the soil layer around Foundation B during compaction.

The F25-ME refrigerated/heated circulator manufactured by Julabo, Inc. operating outside of the centrifuge was connected to Foundation B via the hydraulic

slip ring stack as shown in Figure 5.3. The heat pump has a working temperature range of -28 to 200 °C. An in-line high-capacity cartridge flow pump was attached to the inflow line to supply fluid through the foundations at a rate of 5 ml/s, needed to ensure turbulent flow conditions in the heat exchange tubing and to overcome potential friction losses. Details of the heat exchange fluid used in these tests are presented in McCartney and Rosenberg [MCC 11] and Stewart [STE 12]. The foundation flow valve and bypass flow valve are critical components for controlling the foundation temperature. In order to pre-heat the fluid, the bypass valve can be opened while keeping the foundation flow valve closed. During testing, the foundation flow valve and bypass flow valve can be opened and closed using LabView motor control software to supply the fluid at a given flow rate to reach a desired average temperature in the foundation. The temperatures of the fluid entering and exiting the foundation are monitored using pipe-plug thermocouples, which reflect the energy injected into the foundation.

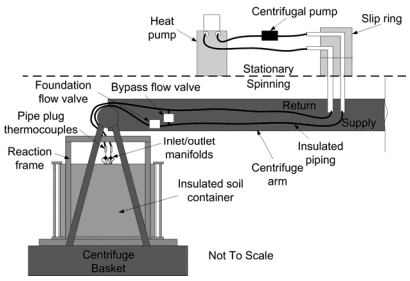


**Figure 5.3:** *Schematic of the container within the loading frame on the centrifuge showing details of the temperature control system*

## 5.5. Centrifuge Modeling Tests for Semi-Floating Foundations

### 5.5.1. *Soil Details*

Soil obtained from the Bonny dam near the Colorado-Kansas border was used in the energy foundation modeling tests presented in this chapter. Information on the compaction curve, shear strength, soil-water retention curve, and shear modulus can be obtained from Stewart [STE 12]. The liquid and plastic limits of the soil measured according to ASTM D 4318 are 26 and 24, and the fines content of this soil is 84%, so this soil classifies as ML (inorganic silt) according to the Unified Soil Classification System (USCS). The silt has a specific gravity $G_s$ of 2.6. The silt was used in these tests as temperature is not expected to lead to changes in soil-pore water interactions (i.e., diffuse double layer effects) due to its low plasticity, while still behaving like a low-permeability material due to its fines content.

Although a wider suite of soil preparation and saturation conditions are under investigation, the tests performed in this study involve soil layers prepared using compaction to permit fast model preparation times and to reach uniform initial unit weight and water content distributions with height at the beginning of the tests. Further, compaction was expected to lead to a stiff soil response that would not lead to significant settlement during centrifuge testing. Foundation A was tested in compacted silt having a gravimetric water content of 13.2% at a dry unit weight of 17.2 kN/m$^3$. Foundation B was tested in compacted silt having a gravimetric water content of 13.6% at a dry unit weight of 17.4 kN/m$^3$. A vibratory hammer with a flat-plate adaptor having a width of 75 mm was used to compact the soil beneath and around the foundations to reach lifts with a final thickness of 75 mm. The centrifuge tests were performed on the soil layers in as-compacted (unsaturated) conditions.

### 5.5.2. *Foundation A: Isothermal Load Tests to Failure*

Each foundation shown in Figure 5.2(a) was tested individually after the soil and foundations had returned to ambient conditions from a previous test. The tests were performed by passing fluid with a controlled temperature through the foundations. The foundations were evaluated for the case that there is no building load applied to the top of the foundation, which means that the foundations were free to expand upwards during heating. They may have also expanded downwards and compressed the soil at the toe, using the friction between the soil and foundation as a reaction. The results for the inlet and outlet temperatures for one of the foundation are shown in Figure 5.4(a). Because there was no instrumentation incorporated into Foundation B, the inlet temperature was assumed to represent that of the foundation. The average temperature of the soil at different radial locations was then permitted to reach a constant value, as shown in Figure 5.4(b). Next, the foundation was loaded to failure using a constant loading displacement rate of 0.08 mm/min as shown in Figure 5.4(c). Load-settlement curves for energy foundations were obtained by plotting the measured load versus head displacement, as shown in Figure 5.4(d). The load settlement curves (in prototype scale) for several other energy foundations without a building load during heating are shown in Figure 5.4(d). Because there was no building load during heating, the increase in capacity with temperature noted in this figure can be attributed in part to the increase in radial stresses during heating due to the differential expansion of the foundation and surrounding soil. This increase in radial stresses leads to an increase in ultimate side shear resistance. The foundations that were heated from 15 to 60 °C then loaded axially to failure experienced an increase in side shear of 40% above that of baseline foundations tested at ambient temperature. A plunging-type failure was noted in the foundations tested under higher temperatures, possibly indicating that the foundation behaved in a more brittle fashion due to the greater lateral stresses induced by expansion of the foundation.

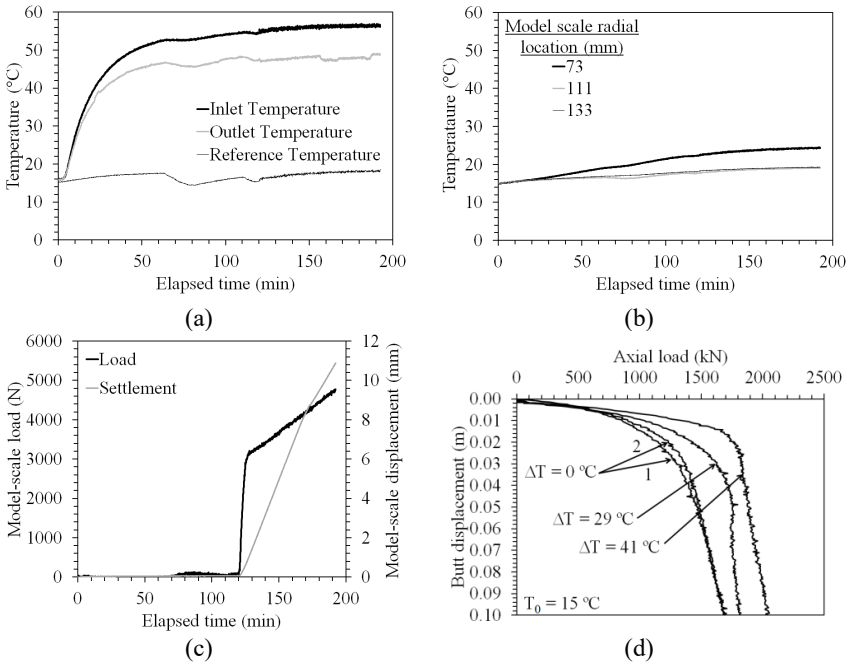


**Figure 5.4:** *Typical results from load-settlement curves on Foundation B for different temperatures: (a) Inlet and outlet fluid temperatures; (b) Soil temperatures; (c) Load-displacement time series; (d) Load-settlement curves for different temperatures [MCC 11]*

As a preliminary evaluation, the ultimate capacities of the foundations heated to different temperatures were evaluated from the load-settlement curves shown in Figure 5.4(d) using Davisson's criterion:

$$Q_{ult} = 0.0038m + 0.01D + QL / AE \qquad [5.3]$$

where D is the foundation diameter in prototype scale and QL/AE is the elastic compression of the foundation. The capacity of the two baseline ($\Delta T = 0$) tests were 1380 kN, while the foundations with changes in temperature of 29 and 41 °C had capacities of 1700 and 1820 kN, respectively.

McCartney et al. [MCC 10] performed similar tests to those shown in Figure 5.4, but evaluated the behavior of foundations heated under application of a building load, maintained in load-control conditions so the foundation was still free to expand upwards. Application of the building load was observed to cause some consolidation

of the soil at the toe of the foundation. After stabilization under the building load, one of the foundations was heated to 50 °C (the centrifuge temperature was constant at 15 °C) then loaded to failure. Another foundation was heated to 50 °C, cooled down to 20 °C, then loaded to failure. The capacities for the test loaded under a temperature of 50 C was 2150, while the capacity of the foundation loaded after cooling was 1640 kN. The capacity of the foundation that was heated and cooled was still greater than that of the baseline test (1380 kN). This is due to consolidation of the soil at the foundation tip, as well as an increase in side shear resistance due to consolidation under the increased radial stresses during heating.

In a load transfer analysis, the mobilization of end bearing with tip displacement can be represented using a Q-z curve. The ordinate of this plot is the normalized end bearing (ratio of mobilized end bearing to ultimate end bearing), and the abscissa is the displacement of the pile toe. Similarly, the mobilization of the side shear with displacement can be represented using a T-z curve. The ordinate of this curve is the normalized side shear (ratio of actual side shear to ultimate side shear), while the abscissa is the relative displacement between the shaft element and surrounding soil. Q-z and T-z curves can be defined using hyperbolic functions, with parameters selected to fit the shapes of the experimental load-settlement curves for the baseline cases [MCC 11]. Additional testing is required to evaluate the impact of temperature on shape of the Q-z and T-z curves. The nonisothermal shear strength results from Uchaipichat and Khalili [UCH 09] indicate that there is a thermal softening effect on the shear strength of soils, emphasizing the need for research in this area.

The other important inputs for a load-transfer analysis are the ultimate side shear and end bearing capacities. The end bearing is not expected to increase substantially with temperature unless the stiffness of the building system provides a reaction resulting in consolidation of the soil at the toe during foundation expansion. Some increase in end bearing likely does occur due to the downward movement of the lower half of the foundation during heating. Until this is better investigated, the ultimate end bearing can be estimated using conventional bearing capacity analyses, as $Q_b = 9A_b c_u$, where 9 is the bearing capacity factor for deep foundations (i.e., a circular or square cross-section and a depth greater than 2 diameters), $c_u$ is the undrained shear strength of the soil under the stress state at the tip of the foundation, and $A_b$ is the cross sectional area of the toe. For the compacted silt evaluated in the centrifuge tests, $c_u$ at the depth of the capacity tests was estimated to be 42 kPa using a value of $c_u/\sigma_v' = 0.265$ and a value of $\sigma_v'$ estimated using a total unit weight of 17.2 kN/m$^3$. The estimated value of $Q_b$ is 990 kN.

As an energy foundation expands laterally into the soil during heating, the soil will compress and the interface shear stress will increase in a drained fashion. The magnitude of increase in radial stress will depend on the thermal gradient as well as the contrast in linear coefficients of thermal expansion of the foundation and soil.

The thermal effects were incorporated into an equation for the drained side shear distribution $Q_s$ by McCartney and Rosenberg [MCC 11], defined as:

$$Q_s = \beta A_s \sigma_v' \left(K_0 + \left(K_p - K_0\right) K_T\right) \tan\phi' \quad [5.4]$$

where β is an empirical reduction factor representing soil-interface behavior, $A_s$ is the side surface area, $\sigma_v'$ is the overburden pressure, $K_0$ is the coefficient of lateral earth pressure at rest (1 – sinϕ'), $K_p$ is the coefficient of passive earth pressure (1+sinϕ')/(1-sinϕ'), and ϕ' is the drained friction angle (29° for the compacted silt). $K_T$ represents mobilization of lateral earth pressure during heating, defined as:

$$K_T = -\kappa \alpha_c \Delta T \left[\left(D/2\right)/0.02L\right] \quad [5.5]$$

where κ is an empirical coefficient representing the soil resistance to expansion of the foundation, $\alpha_T$ is the coefficient of thermal expansion of reinforced concrete (assumed to be -8.5 με/°C), and [(D/2)/0.02L] is a geometric normalizing factor. Eq. 5.5 accounts for the impact of radial expansion of the foundation, but does not account for the upward relative movement of the upper half of the foundation during heating. The load-settlement curve from the load-transfer analysis was first fitted to the baseline case, as shown in Figure 5.5. After modifying the T-z and Q-z curves to obtain the correct shape for the load settlement curve, a value of β of 0.55 gave the best fit for the portion of the curve at small displacements.

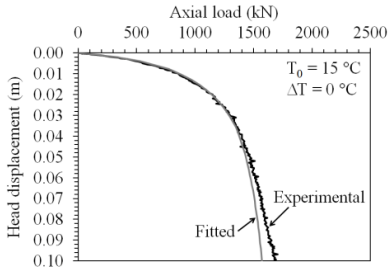


**Figure 5.5:** *Fitted load transfer analysis for isothermal baseline test to define β [MCC 11]*

The fitted load-settlement curve defined for the foundations heated to a temperature of 50 °C is shown in Figure 5.6(a). In this case, a value of κ equal to 65 along with the same value of β = 0.55 was observed to yield a good fit to the experimental curve. The values of β and κ were then used to predict the load settlement curve for the foundation heated to a temperature of 60 °C, shown in Figure 5.6(b) with a maximum error in prediction of 16%.

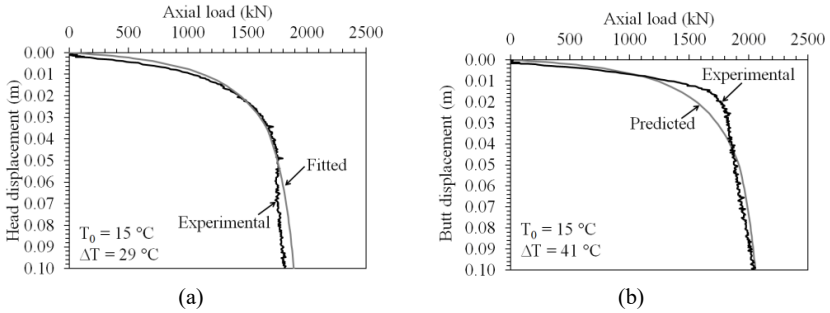


**Figure 5.6:** *Nonisothermal load transfer analysis results [MCC 11]: (a) Fitted analysis to obtain κ; (b) Prediction using fitted value of κ*

### 5.5.3. *Foundation B: Thermo-Mechanical Stress-Strain Modeling*

The first test performed using Foundation B was a load-settlement test under isothermal ambient temperatures. The results from this test are shown in Figure 5.7. The results from this test confirm the assumption from the analysis in the previous section that the side shear distribution is relatively uniform with depth, leading to a decrease in axial strain with depth during loading of the foundation.

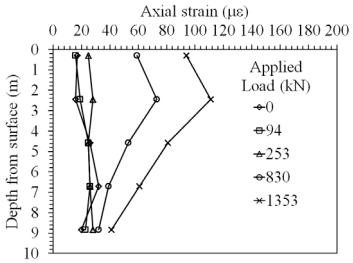


**Figure 5.7:** *Axial strains profiles from a loading test on Foundation B*

A centrifuge test was performed on Foundation A (with embedded strain gages and thermocouples) to assess strain and temperature distributions during cyclic heating. The temperature of the heat exchange fluid and the temperatures at different depths in the foundation are shown in Figures 5.8(a) and 5.8(b). The foundation was heated to a stable value of 32 °C, then was heated further to 40 °C, after which cycles of heating were applied. Profiles of temperature shown in Figure 5.8(c) indicate that the foundation temperature was relatively uniform. The temperature of

the soil surrounding the foundation measured using the dielectric sensors is shown in Figure 5.8(d). The soil temperature lags behind the foundation temperatures due to the heat flow process. Nonetheless, the thermal axial strains were more sensitive to the foundation temperature than the soil temperature.

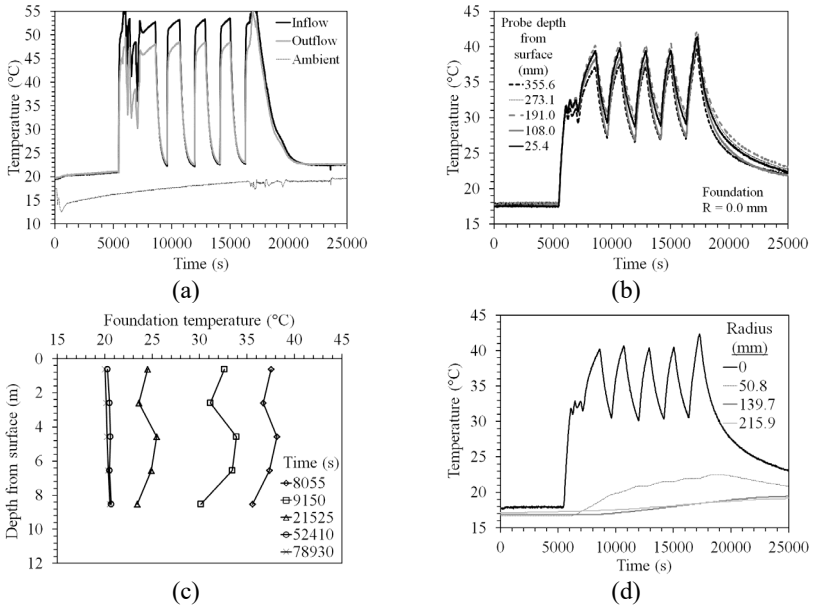


**Figure 5.8:** *Results from cyclic heating test on Foundation B: (a) Inlet-outlet temperatures; (b)Foundation temperatures; (c) Foundation temperature profiles; (d) Soil temperatures*

The time series of axial stress applied to the head of the semi-floating foundation is shown in Figure 5.9(a), along with the average foundation temperature. An axial stress of 150 kPa was maintained except during a malfunction of the load control system after 7000 s. The corresponding mechanical and thermal head displacements are shown in Figure 5.9(b). Although the prototype settlement was nearly 30 mm during the over-loading event, this corresponded to a relatively small settlement in model scale (~1 mm). Examination of the head displacement due to temperature changes (accounting for a slight continued consolidation under the building load) indicates a change in the rate of upward expansion of the foundation head after the over-loading event. After over-loading, the foundation expanded upward by a greater magnitude, likely due to the stiffer soil at the toe of the foundation. After each cooling-heating cycle, the foundation head successively moved downward, due to consolidation and gradual drying of the unsaturated soil around the foundation.

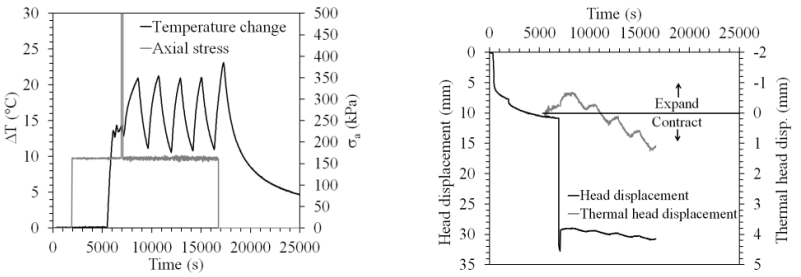


**Figure 5.9:** *(a) Axial stress and temperature; (b) Thermal and mechanical axial displacement*

The thermal strains during the heating process were defined by zeroing the strain readings at the beginning of heating and applying the thermal correction factors obtained from 1-g tests. The thermal axial strains shown in Figure 5.10(a) indicate consistently negative (expansive) strains in the foundation during heating which followed the same trends as the imposed foundation temperatures. The magnitude of the thermal axial strains were consistently lower than the free expansion strain of the foundation $\varepsilon_{T,free}$ defined using Eq. 5.1. The overloading event led to a small strain in the foundation that was recoverable. The centrifuge was stopped in the middle of the final cooling period, leading to spurious strain values. Profiles of axial strain during the initial heating phase are shown in Figure 5.10(b). The largest strains are observed near the foundation head as it is permitted to expand freely under the constant applied load. The smallest strains occur near the center of the foundation, as it is able to expand both upwards and downwards into the soil at the tip.

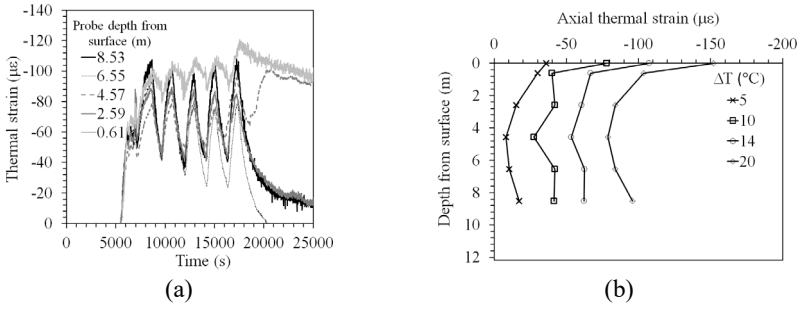


**Figure 5.10:** *Thermal axial strains: (a) Time series; (b) Profile*

The thermal axial displacement profiles obtained by subtracting the integrated strain profile from the measured thermal head displacements are shown in Figure

5.11(a), with negative displacements for upward movement. The location of the zero thermal displacement is referred to as the null-point [KNE 11]. The null point moves downward as the foundation expands and the soil at the toe stiffens, especially after the over-loading event (after ΔT of 14 °C). Thermal stress profiles calculated using Eq. 5.2 are presented in Figure 5.11(b). The maximum thermal stress is located near the middle of the foundation. The soil at the toe provided sufficient restraint that thermal stresses were generated throughout the lower part of the foundation.

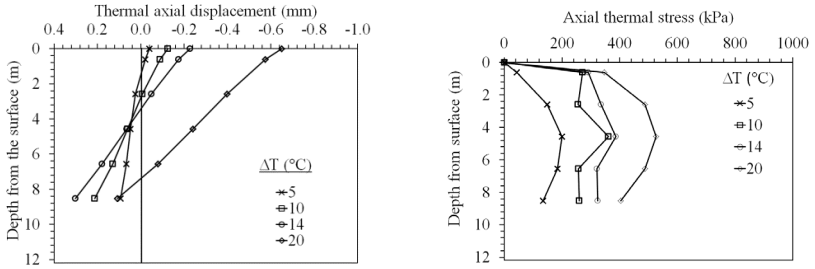


**Figure 5.11:** *Foundation B results: (a) Thermal axial displacement; (b) Thermal axial stress*

## 5.6 Conclusions

The results presented in this chapter indicate that centrifuge modeling can be used to define useful parameters for soil-structure interaction analyses related to energy foundations. The thermal axial strain, displacement, and stress profiles generated in a semi-floating energy foundation in unsaturated silt reveal the importance of end-restraint boundary conditions on the behavior of semi-floating energy foundations. Slight changes in foundation behavior were noted during cycles of heating and cooling, and the mechanisms for this effect should be studied further.

## 5.7 Acknowledgements

Financial support from the National Science Foundation grant CMMI 0928159 is greatly appreciated. The views in this chapter are those of the authors alone.

## 5.8. References

[AMA 12] AMATYA, B., SOGA, K., BOURNE-WEBB, P., AMIS, T., LALOUI, L., "Thermo-mechanical behaviour of energy piles." *Géotechnique*. vol. 62, no. 6, 2012, 503-519.

[BOU 09] BOURNE-WEBB, P., AMATYA, B., SOGA, K., AMIS, T., DAVIDSON, C., PAYNE, P., "Energy pile test at Lambeth College, London: Geotechnical and thermodynamic aspects of pile response to heat cycles." *Géotechnique*. vol. 59, no. 3, 2009, 237–248.

[BRA 98] BRANDL, H., "Energy piles and diaphragm walls for heat transfer from and into the ground." *BAP III*, Ghent, Belgium. October 19-21. Balkema, Rotterdam. 1998, 37–60.

[BRA 06] BRANDL, H., "Energy foundations and other thermo-active ground structures." *Géotechnique*. vol. 56, no. 2, 2006, 81-122.

[ENN 01] ENNIGKEIT, A., KATZENBACH, R., "The double use of piles as foundation and heat exchanging elements." *15th ICSMGE*. Istanbul, Turkey. 2001, 893-896.

[KNE 11] KNELLWOLF, C., PERON, H., LALOUI, L., "Geotechnical analysis of heat exchanger piles." *J. of Geotech. and Geoenv. Eng*. vol. 137, no. 12, 2011, 890-902.

[KO 88] KO, H., "Summary of the state-of-the-art in centrifuge model testing." *Centrifuges in Soil Mechanics*. Craig, James, Scofield, eds. Balkema, 1988, 11-28.

[KRI 04] KRISHNAIAH, S. AND SINGH, D. "Centrifuge modelling of heat migration in soils," *Int. J. of Physical Modelling in Geotechnics.* vol. 4, no. 3, 2004, 39-47.

[LAL 11] LALOUI, L., "In-situ testing of heat exchanger pile." *GeoFrontiers 2011*. Dallas, TX. March 13-16th, 2011. ASCE. 2011, 10 pg.

[LAL 06] LALOUI, L., NUTH, M., VULLIET, L., "Experimental and numerical investigations of the behaviour of a heat exchanger pile." *Int. J. of Numerical and Analytical Methods in Geomechanics*, vol. 30, no. 8, 2006, 763–781.

[MCC 10] MCCARTNEY, J., ROSENBERG, J., SULTANOVA, A. (2010). "Engineering performance of thermo-active foundation systems. *GeoTrends 2010*. ASCE GPP 6. Goss, C., Kerrigan, J., Malamo, J., McCarron, M., Wiltshire, R. eds. 2010, 27-42.

[MCC 11] MCCARTNEY, J., ROSENBERG, J., "Impact of heat exchange on side shear in thermo-active foundations." *GeoFrontiers 2011*. Dallas, TX. March 13-16th, 2011, 10 pg.

[MCC 12] MCCARTNEY, J., MURPHY, K., "Strain Distributions in Full-Scale Energy Foundations." *DFI Journal*. vol. 6, no. 2, 2012, 28-36.

[PLA 12] PLASEIED, N., *Load-Transfer Analysis of Energy Foundations*. M.S. Thesis. University of Colorado Boulder. 2012, 90 pg.

[SAV 88] SAVVIDOU, C., "Centrifuge modelling of heat transfer in soil." *Int. Conference Centrifuge 88*, Corté, ed., Balkema, Rotterdam, 1988, 583-591.

[STE 12] STEWART, M. (2012). *Centrifuge Modeling of Soil-structure Interaction in Energy Foundations*. MS Thesis. University of Colorado Boulder. 110 pg.

[TAY 95] TAYLOR R., *Geotechnical Centrifuge Technology*. Blackie. 1995, 296 p.

[UCH 09] UCHAIPICHAT, A., KHALILI, N., "Experimental investigation of thermo-hydro-mechanical behavior of an unsaturated silt." *Géotechnique.* vol. 59, no. 4, 2009, 339-353.